Highly sensitive piezoelectric micromachined ultrasonic transducer operated in air

Tao Wang[1,2], *Takeshi Kobayashi*[3], *Chengkuo Lee*[1,2] ✉

[1]*Department of Electrical and Computer Engineering, National University of Singapore, Singapore 117581, Singapore*
[2]*Center for Intelligent Sensors and MEMS, National University of Singapore, Singapore 117583, Singapore*
[3]*National Institute of Advanced Industrial Science and Technology (AIST), Tsukuba 305-8564, Japan*
✉ *E-mail: elelc@nus.edu.sg*

Published in Micro & Nano Letters; Received on 3rd May 2016; Accepted on 26th May 2016

Piezoelectric micromachined ultrasonic transducer (pMUT) is gaining increasing research interest. It overcomes the inherent shortcomings of conventional bulk ultrasonic transducers such as acoustic impedance mismatching and poor sensitivity. In addition, pMUT does not require the extremely large input voltage as capacitive micromachined ultrasonic transducer. Therefore the pMUT is potential to be integrated into portable electronics. A pMUT array operated in air using the lead zirconate titanate (PZT) thin film polled by high voltage pulses is realised and fully investigated. The high voltage pulses are found to be more effective for PZT poling, where the piezoelectric constant d_{31} is elevated to 105 pm/V. Benefited from such high performance PZT thin film and optimised structure, the fabricated pMUT (500 × 300 μm) achieves a displacement sensitivity of 807 nm/V at its resonant frequency (482 kHz) without DC offset. Compared with previously reported PZT pMUTs, the sensitivity is superior to them even with a smaller membrane. The in-air transmitting performance is also evaluated. A single pMUT element is able to generate 63.7 dB sound pressure level at 10 mm in air with only 2 V input. The proposed high performance pMUT shows its promise for practical applications in portable electronics.

1. Introduction: As the alternative of bulk ultrasonic transducers, the flexural membrane based micromachined ultrasonic transducers (MUT) are gaining increasing interests from researchers and industries [1–11]. Benefited from the advanced micro-electro-mechanical systems (MEMS) technology, MUT is of miniaturised dimension, lower cost and lower power consumption. In addition, MUT also provides more design flexibility [12], better acoustic impedance matching [13], and the capability of realising 2D transducer array [14]. Based on the transduction mechanism, MUTs can be divided to two types: piezoelectric micromachined ultrasonic transducer (pMUT) and capacitive micromachined ultrasonic transducer (cMUT). Although the cMUT has been well developed in last decades [15], several inherent drawbacks limit its applications [16]. To achieve acceptable sensitivity, an extremely small gap under the flexural membrane is required for a cMUT. Realising such small gap could be very challenging and the yield rate may not be good enough. Furthermore, a very high bias voltage of over 100 V is necessary for cMUT, which may bring in safety issues. Integrating into portable electronics thus becomes very challenging.

The pMUT overcomes the abovementioned inherent drawbacks of cMUT. Its operation voltage can be much lowered as to only several volts. Hence, the pMUT is a promising candidate for practical applications, especially for portable electronics. Varieties of novel applications are emerging. With the pMUTs array, 3D ultrasonic image can be real-time captured without physical scanning [14]. Besides the non-invasive imaging, a miniaturised needle-like pMUT is also developed, which may be eventually put into blood vessels for intravascular imaging [17]. Recently, the fingerprint detection is realised using pMUT [18]. Compared with current optic fingerprint sensors, pMUT consumes significantly lower power, which is of great value for extending the battery lifetime. In addition to the imaging related applications, researchers also have demonstrated airborne gesture recognition, where the pMUT can be integrated to mobile phone [19–22]. The airborne gesture recognition may possibly be the next-generation interacting approach with electronic devices.

Piezoelectric material as the key component largely affects the performance of pMUT. Generally, aluminium nitride (AlN) and lead zirconate titanate (PZT) are the two most popular piezoelectric materials for pMUT. Due to the compatibility with complementary metal-oxide-semiconductor process, AlN based piezoelectric MEMS devices become popular in recent years [23–27]. Nevertheless, PZT has much higher piezoelectric constant d_{31} than AlN, and it is still the best choice to realise high performance pMUT for practical use [28].

In this Letter, we fabricate and fully investigate a PZT based pMUT array, leveraging on our recently reported pulse poling process [29, 30]. The high voltage pulses are found to be more effective than DC voltage for PZT poling, and the piezoelectric constant d_{31} can be elevated to as high as 105 pm/V. Moreover, the voltage pulses with extremely short durations can hardly damage the PZT thin film, which also results in a lower dielectric loss (about 0.06). Benefited from the high performance and low loss PZT thin film and optimised structures, the proposed pMUT shows a displacement sensitivity of 807 nm/V at its resonant frequency (482 kHz). Such sensitivity is superior to other previously reported PZT pMUT even with a smaller membrane. A single pMUT element is able to generate 63.7 dB sound pressure level (SPL) at 10 mm in air with only 2 V input. This pMUT could be potentially used for range finding or gesture recognition in portable electronics.

2. Design considerations: The schematic drawings of the pMUT are illustrated in Fig. 1. The released membrane has the dimension of 500 × 300 μm. 2 μm PZT thin film is employed as the piezoelectric layer and 1 μm SiO_2 is used for isolation. According to previous studies, the position of neutral plane, which is related to the silicon thickness, largely affects the electromechanical coupling [31, 32]. If the neutral plane falls into PZT layer, the lower part of PZT works against the upper part, and this may drastically worsen the pMUT performance. The silicon thickness thus should be carefully chosen. A 3D finite element analysis (FEA) piezoelectric device model is built to study the influence of silicon thickness. Driven by input voltage, the normalised membrane displacement with respect to the silicon thickness is shown in Fig. 2*a*. The maximum displacement can be achieved with 1.8 μm silicon layer. In our previous works, however, 10 μm supporting silicon layer is employed to ensure

doi: 10.1049/mnl.2016.0207

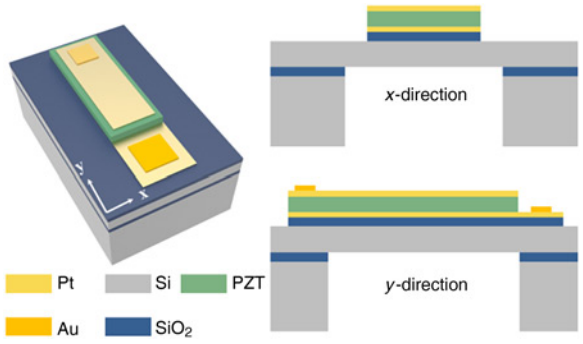

Fig. 1 *Schematic drawings of the proposed high performance pMUT:*
a 3D illustration
b Cross-sectional view of illustration

the yielding rate [28]. As a compromise, 5 µm silicon layer is adopted for the pMUT in this work.

Since the edges of the membrane are fully clamped, membrane curvatures at the centre and edge have the opposite signs when it is deformed [32]. The best efficiency hence cannot be achieved with a fully covered top electrode. To optimise the top electrode, the normalised membrane displacement with respect to the top electrode width is plotted in Fig. 2*b*. It is clearly shown that partially covered top electrode enables a much higher displacement than the fully covered electrode (300 µm width). Largest displacement is achieved at electrode width of 220 µm, and this is the position where the curvature becomes zero. Although the length of top electrode should also be smaller than membrane, the top electrode (*y*-direction) exceeds the membrane because the bonding pad cannot be on the released structure (see Fig. 1*b*). This configuration definitely sacrifices some pMUT performance.

For most of the reported pMUTs, only the top electrode is patterned to simplify the microfabrication processes [33], i.e. the PZT layer, bottom electrode and isolating SiO_2 layer remain as shown in Fig. 2*c*. For the proposed pMUT in this Letter, however, all these layers are etched. Leveraging on the FEA modelling, the performances of the pMUTs with and without etching the PZT/Pt/SiO_2 stack are evaluated. Both models use the optimised parameters with 1 V excitation. As is shown in Fig. 2*c*, the pMUT with etched stack shows superior displacement sensitivity at its resonant frequency, which is about 2.2 times higher than

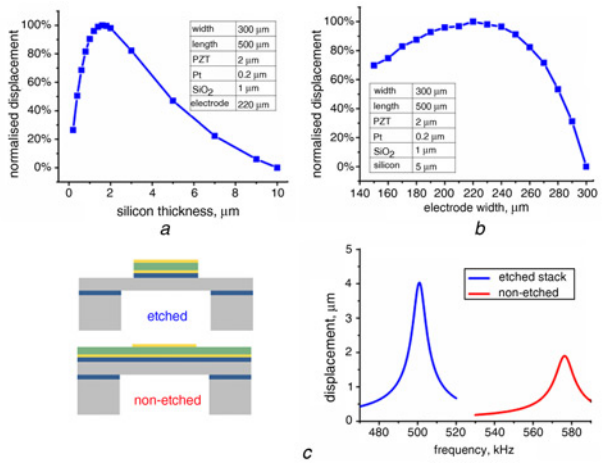

Fig. 2 *Finite elements analysis (FEA) modelling results for pMUT design optimisation*
a Normalised displacement with respect to silicon thickness
b Normalised displacement with respect to top electrode width
c Comparison of the pMUTs with and without the etched PZT/Pt/SiO_2 stack

the non-etched pMUT. Such sensitivity enhancement is probably because the membrane edges are partially free and only the Si layer is clamped. This helps the membrane to vibrate easily and therefore enlarges the displacement sensitivity. The etched pMUT shows a lower resonant frequency, which also implies a smaller elastic constant of the membrane. With all the design considerations, the proposed pMUT is optimised to achieve its best performance.

3. Device fabrication: The micro-fabrication starts from a silicon-on-insulator (SOI) wafer, which has 5 µm device silicon layer, 1 µm buried oxide (BOX) layer and 400 µm handle silicon layer, shown in Fig. 3*a*. A 1 µm SiO_2 thin film is firstly grown on the wafer for isolation. Prior to bottom electrode deposition, a 10 nm Ti adhesion layer is applied. The Pt (200 nm) bottom electrode is then deposited by DC magnetron sputtering. After that, the morphotropic phase boundary composition PZT (Zr/Ti = 52/48, MPB-PZT) thin film is deposited using sol–gel method [34]. The MPB-PZT gives the best piezoelectric constant among all the PZT compositions. A commercially available PZT solution (Kojundo Chemical Co, Japan) is used as a precursor solution. This PZT solution is spin-coated onto the wafer, followed by heating at 120°C and 250°C for drying and pyrolysing. Rapid thermal annealing (RTA) at 650°C is then applied for 2 min to crystallise the PZT thin film. Top electrode is formed by sputtering Pt (200 nm)/Ti (10 nm) on the PZT surface. Fig. 3*b* shows the deposited multilayer stack. The stack is patterned as shown in Fig. 3*c*, using Ar ion milling, wet etching and reactive ion etching (RIE) for etching the Pt/Ti, PZT and SiO_2, respectively. To form the wire bonding pads, a 100 nm Au is deposited by DC magnetron sputtering and patterned by wet etching (Fig. 3*d*). Finally the flexural membrane is released by removing Si substrate and BOX from backside surface using deep reactive ion etching (DRIE), as shown in Fig. 3*e*. The poling process is after all the microfabrication steps are finished, in order

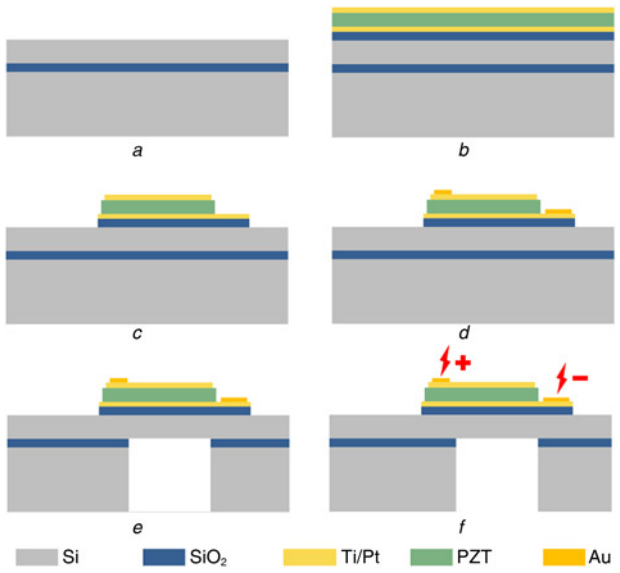

Fig. 3 *Fabrication process flow of the device*
a SOI substrate with 5 µm device silicon layer and 400 µm handle silicon layer
b Deposition of 1 µm SiO_2/10 nm Ti/200 nm Pt/2 µm MPB-PZT/10 nm Ti/200 nm Pt stack. The PZT thin film is deposited by sol–gel method, followed by RTA at 650 °C for crystallisation
c Patterning of the stack. Ar ion milling, wet etching and RIE are for metal, PZT and SiO_2, respectively
d Au (100 nm) wire bonding pads formation
e Backside Si DRIE to release the flexural membrane
f Unipolar pulse poling of PZT thin film at 100 V

to maintain the best piezoelectric performance. The 100 V unipolar voltage pulses (1 kHz triangle voltage pulses with interval of 0.1 s for 10 times) are applied to each device via the bonding pads, shown in Fig. 3*f*.

The as-fabricated pMUT devices are shown in Fig. 4*a* and each die contains 11 pMUT elements. The red dash line in the optical microscope image indicates the released pMUT membrane. The secondary electron microscope (SEM) images are shown in Fig 4*b*. Zigzag edges can be found for the PZT thin film as it is patterned using wet etching. To avoid the possible short circuit between top and bottom electrodes though the PZT thin film, the PZT/Pt/SiO_2 stack is intentionally larger than the top electrode. As the top electrode maintains the optimised 220 µm width, the slightly larger PZT/Pt/SiO_2 stack has minimum reverse effects on the pMUT performance. The cross-sectional view SEM images are shown as well in Fig. 4*c*. It is clearly shown that the top electrode and the PZT/Pt/SiO_2 stack is etched and partially covers the released membrane, which ensures the maximum performance. In addition, the BOX layer is removed completely. According to the simulation result in Fig. 2*a*, any increase in membrane thickness may further lower the pMUT performance. This fabricated pMUT fulfils all the design requirements for the optimised performance.

4. Characterisation and discussions: The pMUT is first characterised using the DHM-R2100 digital holographic microscope from Lyncée Tec Ltd. Fig. 5*a* shows the captured 3D image of one pMUT element. The released membrane looks relatively flat, because the top Pt/Ti electrode is compressively stressed which compensates the tensile stress of the PZT thin film. Details of the stress control are described in our previous study [35]. With the help of the relatively flat membrane, the buckling induced performance degradation can be alleviated [36]. The pMUT is then electrically excited by the stroboscopic module of the holographic microscope with 1 V AC voltage, and the 3D images during motion are captured for analysis. The captured mode shapes are illustrated in Fig. 5*b*, and the displacement sensitivity with respect to frequency is plotted in Fig. 5*c*. The sensitivity is more than 807 nm/V at the resonant frequency (482 kHz), which is a considerably high performance. Table 1 summarises several previously reported PZT based pMUTs. Benefited from the MPB-PZT thin film with high d_{31} and low dielectric loss, as well as the design optimisation, the proposed pMUT shows superior performance to the others even with much smaller membrane dimension. Moreover, the driving voltage of previously reported pMUT has to be high enough (>10 V) to achieve expected displacement. Such high voltage may result in the repolarisation of PZT thin film, and hence those pMUTs employ large DC bias to avoid the repolarisation and performance degradation. For the proposed highly sensitive pMUT, however, the expected displacement can be achieved with rather small driving voltage. Considering the 7 V coercive voltage of the MPB-PZT thin film, a 2–3 V driving voltage can be quite safe for the device. Without the large DC and AC voltage, the proposed pMUT consumes less power and helps to extend its lifetime, which is suitable for integrating to portable electronics.

However, the measured displacement sensitivity is still lower than the prediction by FEA modelling. This over estimation may be mainly attributed to two reasons. First of all, the FEA modelling uses the fixed boundary condition for the membrane edges. Such boundary condition simplifies the model and accelerates the calculation, but does not consider the anchor loss. In fact, the edge is not ideally fixed but slightly moves. Part of the vibration energy of membrane thus propagates into the Si substrate, resulting in lowered displacement sensitivity. The measured lower resonant frequency and lower Q-factor are also due to the non-considered anchor loss. Second, the displacement is very sensitive to the membrane stress. Although the membrane is relatively flat, the non-obvious buckling may still largely hamper the membrane vibration [39, 40]. In addition, the polling process adds extra tensile stress to PZT thin film [32], which makes the situation even worse. Other non-ideal effects during microfabrication process may contribute to the sensitivity degradation as well.

Impedance characterisation is then performed using the Agilent 4294A precision impedance analyser, and the measurement results of a single element are plotted in Fig. 6*a*. Compared with AlN based pMUT, where the impedance is usually several kΩ [24, 41], the PZT based pMUT shows a much low impedance. If seven pMUT elements work together, standard 50 Ω impedance can be achieved which well matches with circuits and coaxial cables. The electromechanical coupling coefficient k_{eff}^2 can be derived from resonant frequency f_r and anti-resonant frequency f_a

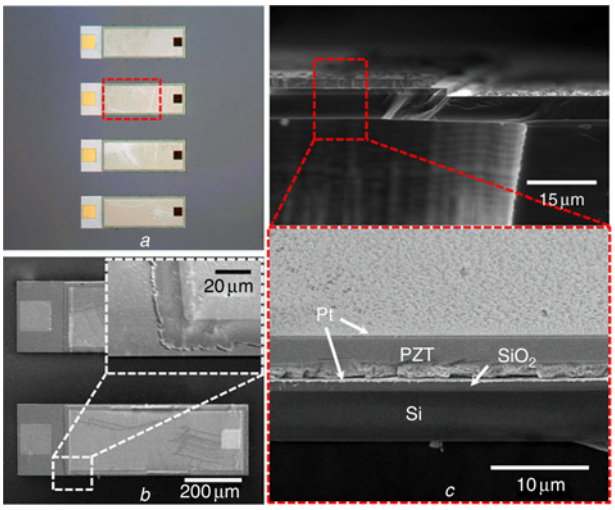

Fig. 4 *As-fabricated pMUT devices*
a Optical microscope (OM) image of the fabricated pMUT. The red dash lines indicate the released membrane
b SEM image of the fabricated pMUT. Top electrode partially covers the membrane
c Cross-sectional view of the SEM image. It is clearly shown the PZT/Pt/SiO_2 stack is etched and the BOX is completely removed. This fabricated pMUT fulfils all the design requirements for the optimised performance

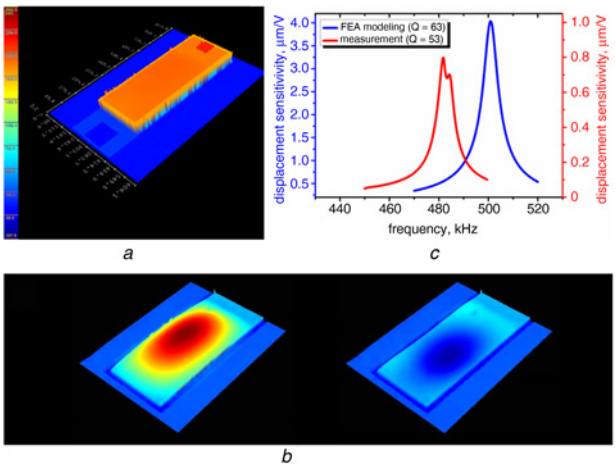

Fig. 5 *Captured 3D image of one pMUT element*
a 3D image of the pMUT, captured by the digital holographic microscope. No obvious membrane buckling can be observed
b 3D mode shape captured during vibration
c Measured displacement sensitivity of the pMUT without DC offset. A 807 nm/V sensitivity is achieved at the resonant frequency (482 kHz), which is considerably high

doi: 10.1049/mnl.2016.0207

Table 1 Comparison of displacement sensitivities of PZT based pMUTs

Device	Dimension, μm	DC offset, V	Resonant Frequency, kHz	Displacement sensitivity, nm/V
Zhu *et al.* [37]	1500 × 1500	30	58	200
Wang *et al.* [38]	2000 × 2000	20	45	83
Muralt *et al.* [32]	1100 (Circ.)	5	49	420
this work	500 × 300	0	482	807

through following relation [33]

$$k_{\text{eff}}^2 = \frac{f_a^2 - f_r^2}{f_a^2} \tag{1}$$

This parameter directly reflects the electrical-mechanical energy conversion efficiency of the device. The in-air k_{eff}^2 is calculated as 1.62%, which is higher than recently reported PZT pMUTs: 1.56% [41], 1.42% [38], 1.29% [8] and 1.12% [33].

As pMUT array, several pMUT elements are simultaneously driven to enhance the transmitted ultrasound pressure. However, if the deviation of their resonant frequencies is too large, the driving frequency may fall into the resonances of only a few elements. As the consequence, the pMUT array cannot achieve its best performance. Thus, the uniformity of the elements is of interest as well. Six pMUT elements from the same die are tested using the digital holographic microscope. Their normalised frequency responses are illustrated in Fig. 6*b*. Because of the well-controlled fabrication processes, these elements show quite good uniformity. Their resonant frequencies are very close, with maximum deviation of only 1.67%. The pMUT in this work exhibit much better uniformity than recently reported work, where the maximum deviation is 8% due to poor control over residual stress [42].

5. In-air transmitting testing: The proposed pMUT, which is of high performance and high uniformity, shows its promise for practical applications in portable electronics. One of the potential applications is the airborne gesture recognition for remote interaction with electronic devices, where the pMUT is used to transmit ultrasound waves. In order to evaluate the transmitting performance of the pMUT, the in-air testing is performed with setups shown in Figs. 7*a* and *b*. An ultrasound microphone (CM16/CMPA externally polarised condenser ultrasound microphone from Avisoft-Bioacoustics, together with the UltrasoundGate 116H data acquisition system) is employed to record the transmitted ultrasound. Before the testing, this

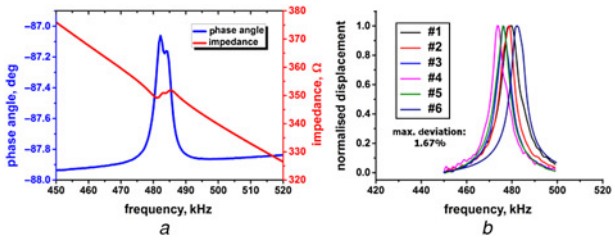

Fig. 6 *Measurement results of a single element*
a Impedance measurement results of the pMUT. The PZT based devices shows relatively low impedance, and standard 50 Ω can be achieved by connecting 7 pMUTs in parallel for impedance match. The electromechanical coupling coefficient is derived from the resonant and anti-resonant frequencies as 1.62%
b Uniformity testing results of the pMUT array. This pMUT array shows quite good uniformity, where the maximum frequency deviation is only 1.67%

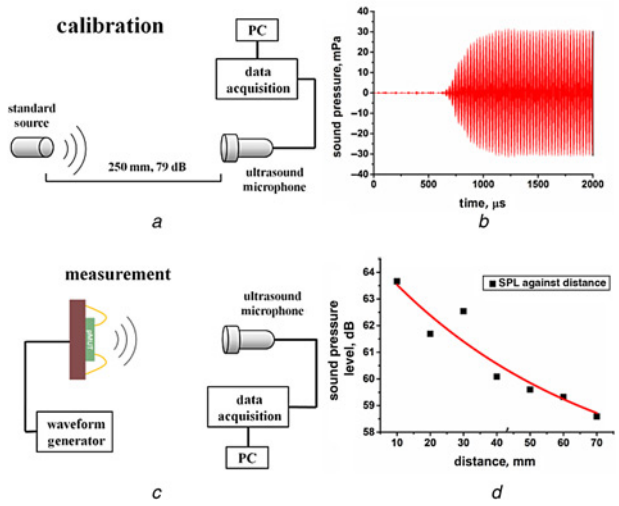

Fig. 7 *In-air testing is performed with setups*
a and *b* Setup for in-air transmitting testing. A standard ultrasound source is used for calibration first, which is able to generate 79 dB SPL at the distance of 250 mm
c Recorded ultrasound transmitted by a single pMUT element at a distance of 10 mm and;
d SPL change with respect to the distance. The SPL drops exponentially, and the deviations at distance of 20 mm and 30 mm are probably due to the standing wave between the pMUT and the microphone

microphone is calibrated first. As is shown in Fig. 7*a*, a standard source is fixed 250 mm away from the microphone. It continuously generates ultrasound waves once switched on, and the SPL at the distance of 250 mm is 79 dB (20 μPa as reference sound pressure in air). The microphone records such ultrasound for 10 s and takes it as the reference for the following testing. The standard source then is replaced by the pMUT under testing, shown in Fig. 7*b*. A single pMUT element is driven by 2 V sinusoidal signal at 482 kHz without DC offset. Such low voltage prevents the unwanted PZT thin film repolarisation and performance degradation. A 31 mPa ultrasound pressure is measured at distance of 10 mm, shown in Fig. 7*c*. The SPL change with respect to distance is measured as well. As is shown in Fig. 7*d*, the SPL decreases exponentially with distance, and 58.5 dB SPL can still be detected at distance of 70 mm. Since air is a highly damped medium, high frequency ultrasound may suffer significant attenuation. Although the 482 kHz frequency of this pMUT may not be low enough for air, the lower frequency can be always achieved by increasing the membrane dimension. Development of the pMUT with lower frequency will be our future works, and the sensitivity of low frequency pMUT would be even higher due to the larger membrane dimension. It is also worth noting that the SPL at 20 and 30 mm largely deviates. This is probably because of the standing wave between the pMUT and microphone, and the microphone located at node or antinode experiences depressed or enhanced ultrasound pressure, respectively.

5. Conclusions: In this Letter, a high performance pMUT is realised. Leveraging on the newly developed pulse poling process, the MPB-PZT thin film has a piezoelectric constant d_{31} as high as 105 pm/V, and low dielectric loss of 0.06. Benefited from the high performance PZT thin film and the optimised pMUT design, the fabricated pMUT exhibits a displacement sensitivity of 807 nm/V at its resonant frequency (482 kHz) with dimension of 500 × 300 μm. Such considerably high sensitivity is achieved with no DC offset. A single pMUT element is able to generate 63.7 dB SPL at 10 mm in air with only 2 V input. The low input voltage not only provides low power consumption, but also prevents the unwanted PZT repolarisation and extends the

pMUT lifetime. The proposed pMUT shows its promise for practical applications in portable electronics.

6. Acknowledgments: This work was supported by the NRF-CRP001-057 Competitive Research Program (CRP) 'Self-Powered Body Sensor Network for Disease Management and Prevention-Oriented Healthcare' under Grant R-263-000-A27-281 from the National Research Foundation, Singapore, and partially supported the Japan Society for the Promotion of Science (JSPS) through the 'Funding Program for World-Leading Innovative R&D on Science and Technology (FIRST Program)', initiated by the Council for Science and Technology Policy (CSTP).

7 References

[1] Khuri-Yakub B.T., Oralkan O.: 'Capacitive micromachined ultrasonic transducers for medical imaging and therapy', *J. Micromech. Microeng.*, 2011, **21**, (5), pp. 54004–54014

[2] Huang Y., Zhuang X., Haeggstrom E.O., *ET AL.*: 'Capacitive micromachined ultrasonic transducers with piston-shaped membranes: fabrication and experimental characterization', *IEEE Trans. Ultrason. Ferroelectr. Freq. Control*, 2009, **56**, (1), pp. 136–145

[3] Yamashita K., Nishiumi T., Arai K., *ET AL.*: 'Intrinsic stress control of sol-gel derived PZT films for buckled diaphragm structures of highly sensitive ultrasonic microsensors', *Procedia Eng.*, 2015, **120**, pp. 1205–1208

[4] Ma J.Q., Hu Y.L., Chen J.J., *ET AL.*: 'Displacement improvement of piezoelectric membrane microactuator by controllable in-plane stress', *Sens. Actuators A Phys.*, 2015, **230**, pp. 45–51

[5] Akhbari S., Sammoura F., Shelton S., *ET AL.*: 'Highly responsive curved aluminum nitride Pmut'. 2014 IEEE 27th Int. Conf. on Micro Electro Mechanical Systems (MEMS), IEEE, 2014

[6] Dausch D.E., Gilchrist K.H., Carlson J.B., *ET AL.*: 'In vivo real-time 3-D intracardiac echo using Pmut arrays', *IEEE Trans. Ultrason. Ferroelectr. Freq. Control*, 2014, **61**, (10), pp. 1754–1764

[7] Mastronardi V.M., Guido F., Amato M., *ET AL.*: 'Piezoelectric ultrasonic transducer based on flexible AlN', *Microelectron. Eng.*, 2014, **121**, pp. 59–63

[8] Jung J., Lee W., Kang W., Hong H., *ET AL.*: 'A top-crossover-to-bottom addressed segmented annular array using piezoelectric micromachined ultrasonic transducers', *J. Micromech. Microeng.*, 2015, **25**, (11), p. 115024

[9] Hajati A., Latev D., Gardner D., *ET AL.*: 'Monolithic ultrasonic integrated circuits based on micromachined semi-ellipsoidal piezoelectric domes', *Appl. Phys. Lett.*, 2013, **103**, (20), p. 202906

[10] Hajati A., Latev D., Gardner D., *ET AL.*: 'Three-dimensional micro electromechanical system piezoelectric ultrasound transducer', *Appl. Phys. Lett.*, 2012, **101**, (25), p. 253101

[11] Chen B.Z., Chu F.T., Liu X.Z., *ET AL.*: 'AlN-based piezoelectric micromachined ultrasonic transducer for photoacoustic imaging', *Appl. Phys. Lett.*, 2013, **103**, (3), p. 031118

[12] Akasheh F., Myers T., Fraser J.D., *ET AL.*: 'Development of piezoelectric micromachined ultrasonic transducers', *Sens. Actuators A Phys.*, 2004, **111**, (2–3), pp. 275–287

[13] Eccardt P.C., Niederer K.: 'Micromachined ultrasound transducers with improved coupling factors from a Cmos compatible process', *Ultrasonics*, 2000, **38**, (1–8), pp. 774–780

[14] Khuri-Yakub B.T., Oralkan O., Kupnik M.: 'Next-gen ultrasound', *IEEE Spectrum*, 2009, **46**, (5), pp. 44–+

[15] Anderson M.J., Hill J.A., Fortunko C.M., *ET AL.*: 'Broadband electrostatic transducers: modeling and experiments', *J. Acoust. Soc. Am.*, 1995, **97**, (1), pp. 262–272

[16] Qiu Y., Gigliotti J.V., Wallace M., *ET AL.*: 'Piezoelectric Micromachined Ultrasound Transducer (Pmut) arrays for integrated sensing, actuation and imaging', *Sensors (Basel)*, 2015, **15**, (4), pp. 8020–8041

[17] Lu Y.P., Heidari A., Horsley D.A.: 'A high fill-factor annular array of high frequency piezoelectric micromachined ultrasonic transducers', *J. Microelectromech. Syst.*, 2015, **24**, (4), pp. 904–913

[18] Tang H., Lu Y., Fung S., *ET AL.*: 'Pulse-echo ultrasonic fingerprint sensor on a chip'. 2015 18th Int. Conf. on Solid-State Sensors, Actuators and Microsystems (TRANSDUCERS), IEEE, 2015

[19] Rozen O., Block S.T., Shelton S.E., *ET AL.*: 'Air-coupled aluminum nitride piezoelectric micromachined ultrasonic transducers at 0.3 Mhz to 0.9 Mhz'. 2015 28th IEEE Int. Conf. on Micro Electro Mechanical Systems (MEMS), 2015

[20] Przybyla R.J., Shelton S.E., Guedes A., *ET AL.*: 'In-air rangefinding with an AlN piezoelectric micromachined ultrasound transducer', *IEEE Sens. J.*, 2011, **11**, (11), pp. 2690–2697

[21] Przybyla R., Flynn A., Jain V., *ET AL.*: 'A micromechanical ultrasonic distance sensor with >1 Meter range'. 2011 16th Int. Solid-State Sensors, Actuators and Microsystems Conf. (TRANSDUCERS) IEEE, 2011

[22] Przybyla R., Izyumin I., Kline M., *ET AL.*: 'An ultrasonic rangefinder based on an AlN piezoelectric micromachined ultrasound transducer'. Sensors, 2010 IEEE, IEEE, 2010

[23] Wang T., Mu X.J., Kropelnicki P., *ET AL.*: 'Viscosity and density decoupling method using a higher order lamb wave sensor', *J. Micromech. Microeng.*, 2014, **24**, (7), p. 075002

[24] Wang T., Lee C.: 'Zero-bending Piezoelectric Micromachined Ultrasonic Transducer (Pmut) with enhanced transmitting performance', *J. Microelectromech. Syst.*, 2015, **24**, (6), pp. 2083–2091

[25] Wang T., Sawada R., Lee C.: 'A Piezoelectric micromachined ultrasonic transducer using piston-like membrane motion', *IEEE Electron Device Lett.*, 2015, **36**, (9), pp. 957–959

[26] Wang T., Mu X.J., Randles A.B., *ET AL.*: 'Diaphragm shape effect on the sensitivity of surface acoustic wave based pressure sensor for harsh environment', *Appl. Phys. Lett.*, 2015, **107**, (12), p. 123501

[27] Wang T., Lee C.: 'Electrically switchable multi-frequency Piezoelectric Micromachined Ultrasonic Transducer (Pmut)'. 2016 IEEE 29th Int. Conf. on Micro Electro Mechanical Systems (MEMS), IEEE, 2016

[28] Wang T., Kobayashi T., Lee C.: 'Micromachined piezoelectric ultrasonic transducer with ultra-wide frequency bandwidth', *Appl. Phys. Lett.*, 2015, **106**, (1), p. 013501

[29] Kobayashi T., Suzuki Y., Makimoto N., *ET AL.*: 'Influence of pulse poling on the piezoelectric property of Pb(Zr0.52,Ti0.48)O3 thin films', *AIP Advances*, 2014, **4**, (11), p. 117116

[30] Kobayashi T., Makimoto N., Suzuki Y., *ET AL.*: 'Effects of bipolar pulse poling on the ferroelectric and piezoelectric properties of tetragonal composition Pb (Zr0.3, Ti0.7) O3 Thin Films on Microelectromechanical Systems Microcantilevers', *JpnJ. Appl. Phys.*, 2013, **52**, (9S1), p. 09KA01

[31] Muralt P., Baborowski J.: 'Micromachined ultrasonic transducers and acoustic sensors based on piezoelectric thin films', *J. Electroceram.*, 2004, **12**, (1–2), pp. 101–108

[32] Muralt P., Ledermann N., Baborowski J., *ET AL.*: 'Piezoelectric Micromachined ultrasonic transducers based on PZT thin films', *IEEE Trans. Ultrason. Ferroelectr. Freq. Control*, 2005, **52**, (12), pp. 2276–2288

[33] Jung J., Kim S., Lee W., *ET AL.*: 'Fabrication of a two-dimensional piezoelectric micromachined ultrasonic transducer array using a top-crossover-to-bottom structure and metal bridge connections', *J. Micromech. Microeng.*, 2013, **23**, (12), p. 125037

[34] Kobayashi T., Ichiki M., Tsaur J., *ET AL.*: 'Effect of multi-coating process on the orientation and microstructure of Lead Zirconate Titanate (PZT) thin films derived by chemical solution deposition', *Thin Solid Films*, 2005, **489**, (1–2), pp. 74–78

[35] Kobayashi T., Ichiki M., Noguchi T., *ET AL.*: 'Deflection of wafers and cantilevers with Pt/Lno/Pzt/Lno/Pt/Ti/SiO_2 multilayered structure', *Thin Solid Films*, 2008, **516**, (16), pp. 5272–5276

[36] Wang T., Lee C.: 'Piezoelectric Micromachined ultrasonic transducer of flat membrane with boosted transmitting performance'. 18th Int. Conf. on Solid-State Sensors, Actuators and Microsystems (TRANSDUCERS), 2015

[37] Zhu H., Mioa J.M., Wang Z.H., *ET AL.*: 'Fabrication of ultrasonic arrays with 7 Mu M PZT thick films as ultrasonic emitter for object detection in air', *Sens. Actuators A Phys.*, 2005, **123–24**, pp. 614–619

[38] Wang Z.H., Miao J.M., Zhu W.G.: 'Micromachined ultrasonic transducers and arrays based on piezoelectric thick film', *Appl. Phys. a-Mater. Sci. Process.*, 2008, **91**, (1), pp. 107–117

[39] Sammoura F., Smyth K., Kim S.-G., *ET AL.*: 'An accurate equivalent circuit for the clamped circular multiple-electrode Pmut with residual stress'. 2013 IEEE Int. Ultrasonics Symp. (IUS), IEEE, 2013

[40] Sammoura F., Smyth K., Bathurst S., *ET AL.*: 'An analytical analysis of the sensitivity of circular piezoelectric micromachined ultrasonic transducers to residual stress'. 2012 IEEE Int. Ultrasonics Symp. (IUS), IEEE, 2012

[41] Lu Y.P., Horsley D.A.: 'Modeling, fabrication, characterization of piezoelectric micromachined ultrasonic transducer arrays based on cavity Soi wafers', *J. Microelectromech. Syst.*, 2015, **24**, (4), pp. 1142–1149

[42] Horsley D.A., Przybyla R.J, Kline M.H., Shelton S.E., Guedes A., Izyumin O., Boser B.E.: 'Piezoelectric micromachined ultrasonic transducers in consumer electronics: the next little thing?'. The 29th IEEE Int. Conf. on Micro Electro Mechanical Systems, 2016

doi: 10.1049/mnl.2016.0207